Scientific Research Publishing

International Journal of Astronomy and Astrophysics, 2023, 13, 61-73
https://www.scirp.org/journal/ijaa
ISSN Online: 2161-4725
ISSN Print: 2161-4717

Transport in Astrophysics: IV. Anomalous Redshift in the Solar System

Lorenzo Zaninetti

Physics Department, Turin, Italy
Email: l.zaninetti@alice.it

How to cite this paper: Zaninetti, L. (2023) Transport in Astrophysics: IV. Anomalous Redshift in the Solar System. *International Journal of Astronomy and Astrophysics*, **13**, 61-73.
https://doi.org/10.4236/ijaa.2023.132004

Received: March 1, 2023
Accepted: June 4, 2023
Published: June 7, 2023

Abstract

The anomalous redshift on the sun's limb and that measured by Pioneer-6 are interesting for the process of absorption of light and the spatial density of matter around the sun. Here we derive a 3D solution for the diffusion equation in the case of the steady state, which is then adopted as the density of the ionized matter around the sun. In order to deal with the observed light's intensity, two integrals along the line of sight are evaluated. Alternatives to the Doppler shift have been considered as mechanisms: a thermal model, a plasma effect, the interaction of a low density electromagnetic wave with an electron and the interaction of light with a low density Fermi gas in standard QED. These four models are compared in the case of the Pioneer-6 signal.

Keywords

Particle Diffusion, Random Walks

1. Introduction

The redshift, z, is defined as

$$z = \frac{\lambda_{obs} - \lambda_{em}}{\lambda_{em}}, \tag{1}$$

with λ_{obs} and λ_{em} denoting respectively the wavelengths of the observed and the emitted e.m. wave, and is usually classified as a Doppler effect. In the case of a redshift generated by another physical mechanism, we speak of an *anomalous redshift*. The first astronomical case to be analysed was the He redshift at the sun's limb, which dates back to 1910 [1] and can be considered a key problem in the Sun's atmosphere. More recent analyses can be found in [2] [3] [4] [5]. The shift of the absorption lines is modeled by different physical mechanisms: a turbulent model for the Sun's atmosphere [6], an atomic model which uses the

Lennard-Jones potential and standard photospheric models [7], a secondary radiation due to bremsstrahlung produced by the transfer of momentum of the solar photons to the electrons of the atoms of the solar atmosphere [8], and a model based on the photons of light losing energy due to interaction with electrons [9]. The above models suggest that at the moment of writing there is no single explanation for the shift of the absorption lines. The second astronomical case here analysed date back to 1969 and is the anomalous redshift at 2292 MHz from Pioneer-6 [10]. Starting from 1971 and up to 2013, different models have been used to analyse this anomalous redshift: radial currents in the solar atmosphere [11] [12] [13] [14], the interaction of the photons with matter [15] and the interaction of light with a low density Fermi gas in standard quantum electrodynamics (QED) [16]. In the period from 2014 up to now the following models have been considered for the anomalous redshift at 2292 MHz: the losses to electromagnetic waves when the electric component accelerates the electrons in the sun's atmosphere [17] and the interaction of the radio signal with the electron-dense solar corona in the framework of New Tired Light (NTL) [18]. Also in the case of Pioneer-6, there does not exist a unique model for the shift in frequency of communication. Some questions have not yet been analysed:

1) Can the radial profile in density of the 3D diffusion explain the decrease in density around the sun?

2) Can we integrate the above diffusion profile along the line of sight?

3) Can we compare different models for the anomalous redshift of the sun?

In order to answer the above questions, Section 2 reviews the relativistic formulae for the Doppler and gravitational redshifts, Section 3 reviews some existing models for the anomalous redshift, such as the photon-matter interaction, the plasma effect, the interaction of a low density electromagnetic wave with an electron and the interaction of light with a low density Fermi gas in standard QED. Section 4 sets up the steady state diffusion in 3D and derives two integrals along the line of sight. Section 5 applies the new results to the anomalous redshift measured on the solar limb and to that connected with Pioneer-6.

2. Relativistic Effects

In the framework of special relativity (SR), we analyse the case in which the receiver is at rest and the source is emitting light with an angle θ with respect to the relative motion. The frequency observed by the receiver, ν, is reduced from ν_0 to

$$\frac{\nu}{\nu_0}=\frac{\sqrt{1-\beta^2}}{1-\beta\cos(\theta)}, \tag{2}$$

where $\beta=\frac{v}{c}$, v is the absolute velocity of the source, and c is the speed of light, see Formula (14.5) in [19]. The relativistic redshift in SR is

$$z=-\frac{\beta\cos(\theta)+\sqrt{-\beta^2+1}-1}{\sqrt{-\beta^2+1}}, \tag{3}$$

and a Taylor expansion up to order 3 in β gives

$$z = -\frac{2\beta\left(\left(\cos^2(\theta)\right)\beta - \frac{\beta}{2} + \cos(\theta)\right)}{2 + 2\left(\cos^2(\theta)\right)\beta^2 + 2\beta\cos(\theta) - \beta^2}. \tag{4}$$

The above equation in the case of $\theta = 90$ deg, transverse motion, gives

$$z = \frac{\beta^2}{2}, \tag{5}$$

and in the case of $\theta = 180$ deg, radial motion, gives

$$z = \beta + \frac{1}{2}\beta^2. \tag{6}$$

In general relativity (GR), the gravitational redshift for the sun is

$$z \approx \frac{GM}{Rc^2} = 2.122 \times 10^{-6}, \tag{7}$$

where G is the Newtonian constant of gravitation, M is the mass of the sun, R is the radius of the sun and c is the speed of light in vacuum, see Formula (5.485) in [20] and see [21] for an historical derivation.

3. Anomalous Redshift

This section reports the adopted statistics and reviews 4 different mechanisms for the anomalous redshift.

3.1. Statistics

The merit function χ^2 is computed according to the formula

$$\chi^2 = \sum_{i=1}^{n} \frac{(T_i - O_i)^2}{O_i}, \tag{8}$$

where n is the number of elements of the sample, T_i is the theoretical value, and O_i is the experimental datum.

3.2. Models

The first mechanism is for reference and is due to the interaction between photons and matter. We start from the two equations on page 170 of [15]

$$T^3 = \frac{T_\odot^3 \omega}{4\pi}, \tag{9}$$

and

$$\frac{\omega}{4\pi} = \frac{1}{2} - \frac{\sqrt{1 - \frac{R_\odot^2}{r^2}}}{2}, \tag{10}$$

where $R_\odot$ is the radius of the sun, T is the temperature at distance r, $T_\odot$ is the temperature at distance $R_\odot$ and ω the considered solid angle. On introducing

$\frac{R_\odot}{r}=\frac{\sin(\text{theta})}{d}$, Equation (2) of [15] for the redshift becomes

$$z=A\left(\int_{-\frac{\pi}{2}}^{\frac{\pi}{2}}-\frac{T_\odot^3\left(-1+\sqrt{1-\frac{\sin^2(\theta)}{d^2}}\right)\pi}{2\pi}\mathrm{d}\theta\right), \tag{11}$$

where A is a constant. An analytical expression for the above integral is

$$z=-\frac{AT_\odot^3\pi\left(-\pi+2E\left(\frac{1}{d}\right)\right)}{2\pi}, \tag{12}$$

where $E(x)$ is the complete elliptic integral of the second kind which according to [22] is

$$E(x)=E(1,x), \tag{13}$$

where $E(z,y)$ is the incomplete elliptic integral of the second kind

$$E(z,y)=\int_0^z\frac{\sqrt{-y^2t^2+1}}{\sqrt{-t^2+1}}\mathrm{d}t. \tag{14}$$

A truncated series expansion of Equation (12) of order 3 with respect to the variable d about the point 1 is

$$\begin{aligned}z=&\frac{AT_\odot^3\pi(\pi-2)}{2\pi}+\frac{AT_\odot^3\pi(-3\ln(2)+\ln(d-1)+1)(d-1)}{2\pi}\\&+\frac{AT_\odot^3\pi\left(\frac{9\ln(2)}{4}-\frac{3\ln(d-1)}{4}-\frac{11}{8}\right)(d-1)^2}{2\pi}.\end{aligned} \tag{15}$$

The maximum percentage error of the above expansion is $\delta\approx 20\%$ in the interval $1<d<1.7$ and we should go to order 12 in order to have $\delta\approx 1\%$. An asymptotic expansion of Equation (12) with respect to the variable d is

$$z=\frac{AT_\odot^3\pi^2}{8\pi d^2}+\frac{3AT_\odot^3\pi^2}{128\pi d^4}. \tag{16}$$

The maximum percentage error of the above expansion is $\delta\approx 1\%$ in the interval $1.7<d<10$. The second case is an analysis of a plasma effect. In the framework of photons which penetrate a hot, sparse electron plasma, it is possible to derive a formula for the redshift

$$\ln(1+z)=3.326\times 10^{-25}\int_0^R N_e\mathrm{d}x+\frac{\gamma_i-\gamma_0}{\xi\omega}, \tag{17}$$

where γ_i is the initial photon width, γ_0 is the final photon width, ω is the photon frequency, ξ is an adjustment factor and N_e is the number of plasma electrons per cm^3, see Equation (20) in [23] or Equation (29) in [24]. The second term of Equation (17) is a small correction to the first term and therefore we have a simple expression for the plasma redshift in the CGS system:

$$\ln(1+z)=3.326\times10^{-25}\int_0^R N_e \mathrm{d}x. \tag{18}$$

The third mechanism is given by the interaction of a low density electromagnetic wave with an electron, see the equation on page 3 in [25], which in the SI system yields the following redshift

$$z=w\int_0^D n_e \mathrm{d}s, \tag{19}$$

with

$$w=\frac{3q_e^4\mu_0}{512\pi m_e^2}=2.33\times10^{-30}\ \mathrm{m}^2, \tag{20}$$

where q_e is the charge of the electron, μ_0 is the magnetic permeability of the vacuum, and m_e is the mass of the electron.

The fourth mechanism is given by the interaction of light with a low density Fermi gas in standard QED, which yields the following redshift

$$z=\frac{3}{400000d^5}+\frac{1}{5000000d}, \tag{21}$$

see the last formula on page 282 in [16].

4. Diffusion from the Sun

Here we assume that the concentration of ionized particles, $C(r,t)$, diffuses away from the surface of the sun according to Fick's second law in 3D

$$\frac{\partial}{\partial t}C(r,t)=\frac{D\left(\frac{\partial}{\partial r}\left(r^2\left(\frac{\partial}{\partial r}C(r,t)\right)\right)\right)}{r^2}, \tag{22}$$

where D is the diffusion coefficient, t is the time and r is the radius. This partial differential Equation (PDE) in the stationary state becomes an ordinary differential Equation (ODE):

$$\frac{D\left(2r\left(\frac{\mathrm{d}}{\mathrm{d}r}C(r)\right)+r^2\left(\frac{\mathrm{d}^2}{\mathrm{d}r^2}C(r)\right)\right)}{r^2}=0. \tag{23}$$

The boundary conditions are assumed to be $C(b)=C_m$ and $C(c)=0$ and the solution of this ODE is

$$C(r)=-\frac{C_m b(c-r)}{(b-c)r}. \tag{24}$$

We are now interested in the integral $I(x,y)=\int C(x,y)\mathrm{d}x$ along a line of sight as shown in **Figure 1**.

We now consider a circular section of the diffusing sphere and make the substitution $r=\sqrt{x^2+y^2}$. We now evaluate two integrals which cover different ranges of the variable y. The first integral, I_{bc}, is taken over the interval $b<y<c$ and is doubled for symmetry, or in other words is taken outside the radius of the sun

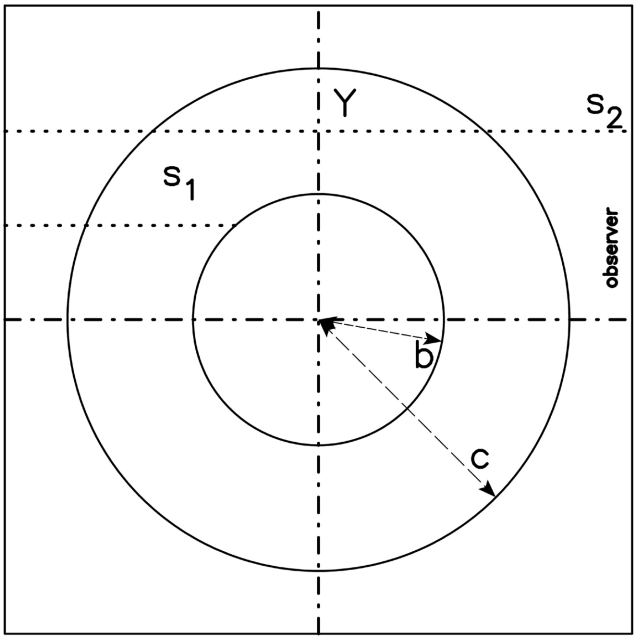

Figure 1. The two circles (sections of spheres) with radius of the sun, *b*, and radius of the end of diffusion, *c*, are represented by a full line. The observer is situated along the *x* direction, and two dotted lines of sight are indicated.

$$I_{bc}=\int_0^{\sqrt{c^2-y^2}} C(x,y)\,\mathrm{d}x = -\frac{2C_m b\left(-\sqrt{c^2-y^2}+c\,\mathrm{arcsinh}\left(\frac{\sqrt{c^2-y^2}}{y}\right)\right)}{b-c};\quad b<y<c, \tag{25}$$

and the second integral, I_{0b}, is taken over the interval $0<y<b$, or in other words is taken from the surface of the sun to the end of the diffusion

$$I_{0b}=\int_{\sqrt{b^2-y^2}}^{\sqrt{c^2-y^2}} C(x,y)\,\mathrm{d}x = \frac{bC_m\left(c\,\mathrm{arcsinh}\left(\frac{\sqrt{b^2-y^2}}{y}\right)-c\,\mathrm{arcsinh}\left(\frac{\sqrt{c^2-y^2}}{y}\right)-\sqrt{b^2-y^2}+\sqrt{c^2-y^2}\right)}{b-c};\quad 0<y<b. \tag{26}$$

A typical result for this integration is reported in **Figure 2**.

In order to parametrize the redshift as a function of the distance in the logarithmic case we fix

$$\ln(1+z_{0b})=A*I_{0b}, \tag{27}$$

where A is a constant and z_{0b} the redshift in the interval $0<y<b$. The redshift is therefore

$$z_{0b}=\mathrm{e}^{\frac{AbC_m\left(c\,\mathrm{arcsinh}\left(\frac{\sqrt{b^2-y^2}}{y}\right)-c\,\mathrm{arcsinh}\left(\frac{\sqrt{c^2-y^2}}{y}\right)-\sqrt{b^2-y^2}+\sqrt{c^2-y^2}\right)}{b-c}}-1, \tag{28}$$

and in an analogous way introducing z_{bc} as the redshift in the interval $b<y<c$

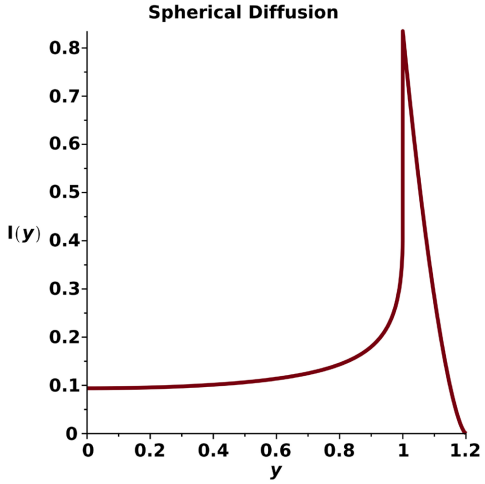

Figure 2. Behaviour of the intensity $I(y)$ exhibited by I_{0b} and I_{bc} as functions of the distance from the centre when $C_m = 1$, $b = 1$ and $c = \frac{6}{5}$.

$$z_{bc} = \mathrm{e}^{\frac{AbC_m\left(c\,\mathrm{arcsinh}\left(\frac{\sqrt{b^2-y^2}}{y}\right)-c\,\mathrm{arcsinh}\left(\frac{\sqrt{c^2-y^2}}{y}\right)-\sqrt{b^2-y^2}+\sqrt{c^2-y^2}\right)}{b-c}}-1. \quad (29)$$

Conversely, in order to parametrize the redshift as a function of the distance in the linear case we fix

$$z = B * I_{0b}, \quad (30)$$

where B is a constant. The redshift is therefore

$$z_{0b} = \frac{BbC_m\left(c\,\mathrm{arcsinh}\left(\frac{\sqrt{b^2-y^2}}{y}\right)-c\,\mathrm{arcsinh}\left(\frac{\sqrt{c^2-y^2}}{y}\right)-\sqrt{b^2-y^2}+\sqrt{c^2-y^2}\right)}{b-c}, \quad (31)$$

and in an analogous way

$$z_{bc} = -\frac{2BC_m b\left(-\sqrt{c^2-y^2}+c\,\mathrm{arcsinh}\left(\frac{\sqrt{c^2-y^2}}{y}\right)\right)}{b-c}. \quad (32)$$

5. Astrophysical Applications

Here we apply the new formulae to the Fraunhofer lines at the sun's limb and to the 2292 MHz radio data from Pioneer-6.

5.1. The Sun's Lines

The redshift of the Fraunhofer spectral absorption lines varies from the centre to the limb of the sun and has been the subject of research. As an example, we analysed the data of [2] and [3] that can be found in Table 3 of [23]. **Figure 3** compares the experimental data with the theoretical curve as given by the plasma-redshift theory with a logarithmic expression for the redshift, see Equation (28).

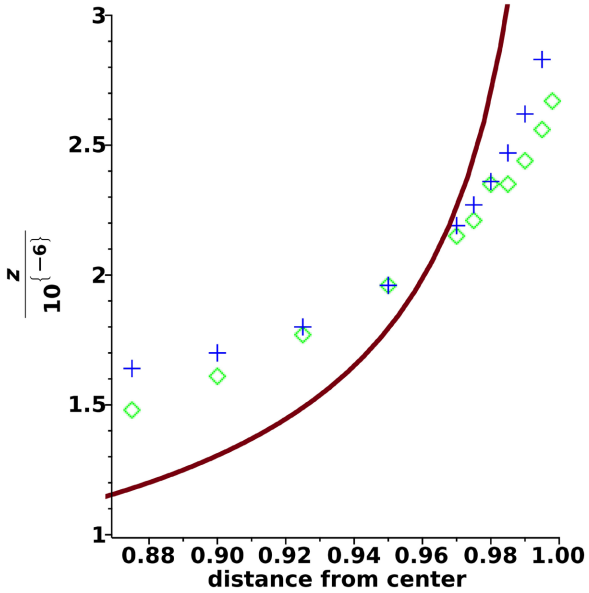

Figure 3. Experimental measurements by [3] (blue crosses) and by [2] (green diamonds) with redshift expressed in 10^{-6} units. Theoretical curve as given by Equation (28) with $b=1$, $c=b+b/100$ (red line), $A=3.326\times10^{-25}$ in CGS and $C_m=N_e=5\times10^9\frac{1}{\text{cm}^3}$.

Figure 4 compares the experimental data with the theoretical curve as given by the interaction of a low density electromagnetic wave with an electron with a linear expression for the redshift, see Equation (31).

Figure 5 compares the experimental data with the theoretical curve as given by the relativistic Doppler model for the redshift, see Equation (4), where the variable $-\cos(\theta)$ has been substituted by the distance from the centre to a given position expressed in solar units. The above relativistic Doppler model is only valid in the presence of a circular velocity at the equator of the sun and in the interval of distance in solar units $[0,1]$. The χ^2 of the three models for the three sets of data is reported in **Table 1**.

5.2. Pioneer-6 Anomalous Redshift

The occultation by the sun of the radio signals at 2292 MHz from Pioneer-6 was observed by [10]. The above data were analysed as redshift versus distance from the sun, see Figure 4 in [15], and explained as an interaction between incident transverse photons and light neutral bosons emitted by the sun. **Figure 6** reports the observed data as well the theoretical analytical curve for the photon-matter interaction, the model of reference, with the χ^2 reported in **Table 2**.

Figure 7 compares the Pioneer-6 data with the theoretical curve as given by the plasma-redshift theory with a logarithmic expression for the redshift, see Equation (29), with χ^2 as in **Table 2**.

Figure 8 compares the Pioneer-6 data with the theoretical curve as given by the interaction of a low density electromagnetic wave with an electron with a linear expression for the redshift, see Equation (32), with χ^2 as in **Table 2**.

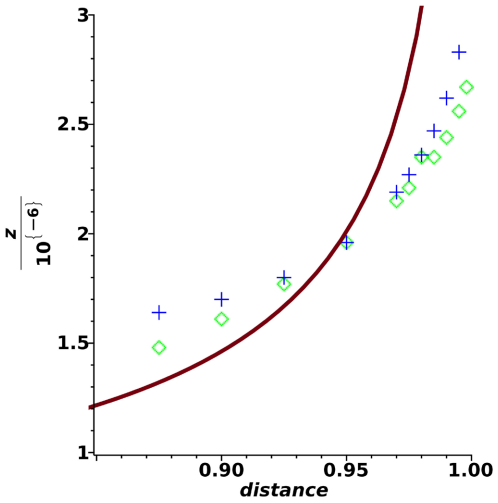

Figure 4. Experimental measurements by [3] (blue crosses) and by [2] (green diamonds) with redshift expressed in 10^{-6} units. Theoretical curve as given by Equation (31) with $b=1$, $c=b+b/100$ (red line), $B=2.33\times10^{-30}$ in SI and $C_m=N_e=0.8\times10^{17}\frac{1}{\mathrm{m}^3}$.

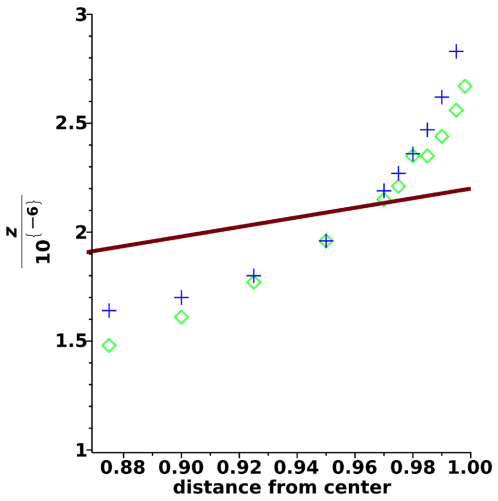

Figure 5. Experimental measurements by [3] (blue crosses) and by [2] (green diamonds) with redshift expressed in 10^{-6} units. Theoretical curve for the Doppler model as given by Equation (4) with $\beta=2.2\times10^{-6}$.

Table 1. Numerical values of χ^2 for the sun.

Involved Physics	Adam (1959) data	Higgs (1960) data
Plasma Physics	2.65	1.69
EM-electron	4.21	2.82
Doppler Effect	0.157	0.23

Figure 9 compares the Pioneer-6 data with the theoretical curve as given by the interaction of light with a low density Fermi gas in standard QED, see Equation (21), with χ^2 as in Table 2.

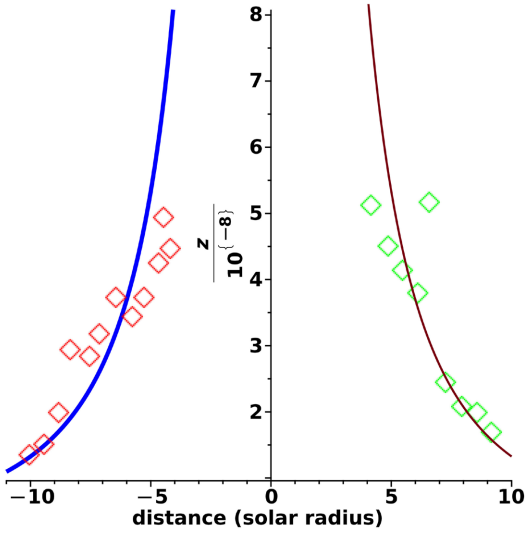

Figure 6. Experimental measurements of the redshift, expressed in 10^{-8} units, of the Pioneer-6 signals (green and red diamonds). Theoretical analytical curve of the photon-matter interaction as given by Equation (12) with $A = 2.5 \times 10^{-28}$ (blue and red line).

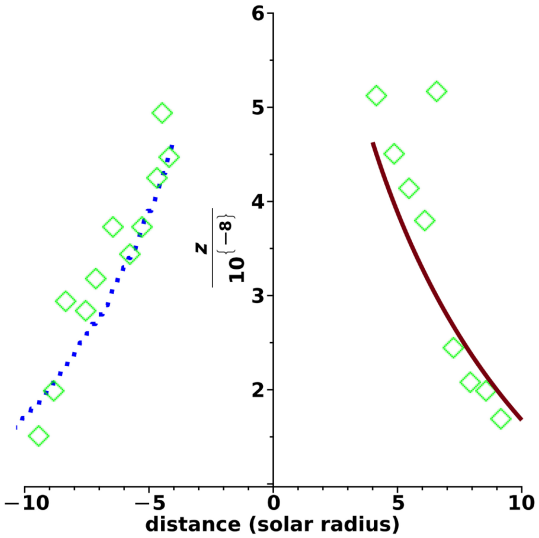

Figure 7. Experimental measurements of the redshift, expressed in 10^{-8} units, of the Pioneer-6 signals (green diamonds). Theoretical curve as given by Equation (29) with $b = 1$, $c = b + 20 \times b$ (red full line and blue dotted line), $A = 3.326 \times 10^{-25}$ in CGS and $C_m = N_e = 7 \times 10^5 \frac{1}{\text{cm}^3}$.

Table 2. Numerical values of χ^2 for the Pioneer-6 signal.

Involved Physics	left data	right data
Photon-Matter	0.33	0.51
Plasma-Physics	0.28	0.3
EM-electron	0.22	0.27
QED	0.49	0.37

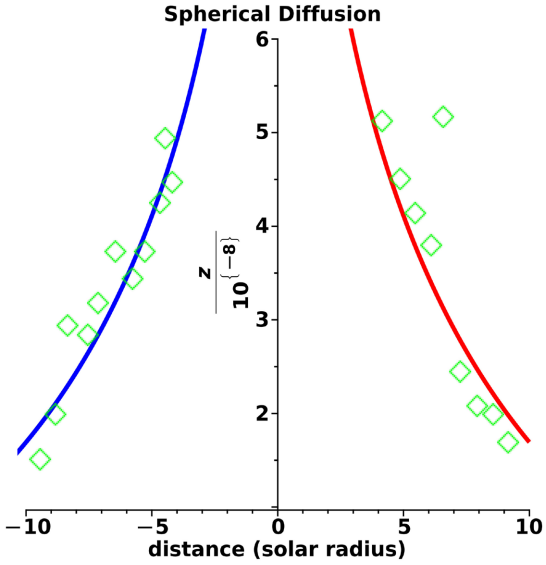

Figure 8. Experimental measurements of the redshift, expressed in 10^{-8} units, of the Pioneer-6 signals (green diamonds). Theoretical curve as given by Equation (32) with $b=1$, $c=b+20\times b$ (red and blue line), $B=2.33\times10^{-30}$ in SI and $C_m=N_e=1.1\times10^{13}\,\frac{1}{\mathrm{m}^3}$.

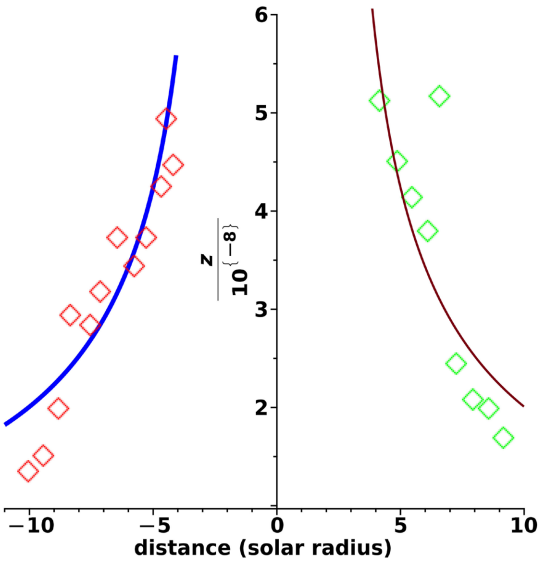

Figure 9. Experimental measurements of the redshift, expressed in 10^{-8} units, of the Pioneer-6 signals (green diamonds). Theoretical curve in the framework of QED as given by Equation (21).

6. Conclusions

Diffusion with stationary state

A solution for the 3D steady state diffusion was presented, see Equation (24). Two new integrals were derived along two different regions of sight, see Equations (25) and (26). These integrals allow deriving 4 new expressions for the anomalous redshift in the logarithmic case, see Equations (28) and (29), and in the linear case, see Equations (31) and (32).

Astrophysical fits

In the case of the anomalous redshift lines at the sun's limb, the best results are obtained by the Doppler shift, see Table 1. Unfortunately, the Doppler shift in the model here suggested presents a linear rather than a curved behaviour, see Figure 5, and in the opposite range of distance is blue-shifted rather than red-shifted. In the case of the anomalous redshift for the Pioneer-6 signals, the best results are obtained by the interaction of the EM wave with matter, followed by the plasma physics effect, see Table 2. The two historical models, the thermal photon-matter interaction and the QED model, produce a bigger χ^2.

Conflicts of Interest

The author declares no conflicts of interest regarding the publication of this paper.

References

[1] Adams, W.S. (1910) An Investigation of the Displacements of the Spectrum Lines at the Sun's Limb. *Astrophysical Journal*, **31**, 30-61. https://doi.org/10.1086/141722

[2] Adam, M.G. (1959) A New Determination of the Centre to Limb Change in Solar Wave-Lengths. *MNRAS*, **119**, 460-474. https://doi.org/10.1093/mnras/119.5.460

[3] Higgs, L.A. (1960) The Solar Red-Shift. *MNRAS*, **121**, 421-435. https://doi.org/10.1093/mnras/121.5.421

[4] Appenzeller, I. and Schröter, E.H. (1967) Center-to-Limb Variations of the Intensity and the Wavelength of Several Fraunhofer Lines along the SUN's Polar and Equatorial Diameter. *Astrophysical Journal*, **147**, 1100. https://doi.org/10.1086/149098

[5] Salman-Zade, R.K. (1969) Limb Effect of the Fraunhofer Lines in the Solar Spectrum. *Soviet Astronomy*, **13**, 466.

[6] Allen, C.W. (1949) Centre-Limb Variations of Fraunhofer Line-Breadths and Intensities. *MNRAS*, **109**, 343. https://doi.org/10.1093/mnras/109.3.343

[7] Hart, M.H. (1974) An Explanation of the Solar Limb Shift. *Astrophysical Journal*, **187**, 393-401. https://doi.org/10.1086/152645

[8] Marmet, P. (1989) Red Shift of Spectral Lines in the Sun's Chromosphere. *IEEE Transactions on Plasma Science*, **17**, 238-243. https://doi.org/10.1109/27.24630

[9] Trinchera, A. (2020) Redshift Anomaly on the Solar Disk as Multiple Interactions between Photons and Electrons. *Journal of High Energy Physics, Gravitation and Cosmology*, **7**, 1-51. https://doi.org/10.4236/jhepgc.2021.71001

[10] Goldstein, R.M. (1969) Superior Conjunction of Pioneer 6. *Science*, **166**, 598-601. https://doi.org/10.1126/science.166.3905.598

[11] Ferencz, C. and Tarcsai, G. (1970) A New Experimental Possibility of Investigating the Solar Corona: Frequency Measurements on Radio Sources When Occultated by the Sun. *Planetary and Space Science*, **18**, 1213-1223. https://doi.org/10.1016/0032-0633(70)90213-8

[12] Ferencz, C. and Tarcsai, G. (1971) Theoretical Explanation of the Solar Limb Effect *Planetary and Space Science*, **19**, 659-667. https://doi.org/10.1016/0032-0633(71)90058-4

[13] Ferencz, C. (1971) Interaction of Gravitational and Electromagnetic Fields or Another Effect? *Nature*, **233**, 404-406. https://doi.org/10.1038/233404a0

[14] Ferencz, C. (1974) Redshift during Pioneer-6 Solar Occultation—Unexplained or Predicted. *Nature*, **252**, 615. https://doi.org/10.1038/252615a0

[15] Merat, P., Pecker, J.C. and Vigier, J.P. (1974) Possible Interpretation of an Anomalous Redsbift Observed on the 2292 MHz Line Emitted by Pioneer-6 in the Close Vicinity of the Solar Limb. *Astronomy & Astrophysics*, **30**, 167-174.

[16] Accardi, L., Laio, A., Lu, Y. and Rizzi, G. (1995) A Third Hypothesis on the Origin of the Redshift: Application to the Pioneer 6 Data. *Physics Letters A*, **209**, 277-284. https://doi.org/10.1016/0375-9601(95)00868-3

[17] Weidner, H. (2014) Pioneer 6 Anomalous Redshift near the Sun.

[18] Trinchera, A. (2021) Redshift Anomaly of the 2292 MHz Radio Signal Emitted by the Pioneer-6 Space Probe as Multiple Interactions with Photo-Ionized Electrons in the Solar Corona. *Journal of High Energy Physics, Gravitation and Cosmology*, **7**, 1107-1156. https://doi.org/10.4236/jhepgc.2021.73066

[19] Freund, J. (2008) Special Relativity for Beginners: A Textbook for Undergraduates. World Scientific Press, Singapore. https://doi.org/10.1142/6601

[20] Lang, K.R. (1999) Astrophysical Formulae. Third Edition, Springer, New York. https://doi.org/10.1007/978-3-662-21639-2

[21] Valente, M.B. (2018) Einstein's Redshift Derivations: Its History from 1907 to 1921. *Circumscribere*, **22**, 1-16. https://doi.org/10.23925/1980-7651.2018v22;1-16

[22] Olver, F.W.J., Lozier, D.W., Boisvert, R.F. and Clark, C.W. (2010) NIST Handbook of Mathematical Functions. Cambridge University Press, Cambridge.

[23] Brynjolfsson, A. (2004) Redshift of Photons Penetrating a Hot Plasma.

[24] Brynjolfsson, A. (2009) Plasma-Redshift Cosmology: A Review. In: Potter, F., Ed., 2*nd Crisis in Cosmology Conference*, Vol. 413 of Astronomical Society of the Pacific Conference Series, Astronomical Society of the Pacific, San Francisco, 169-189.

[25] Weidner, H. (2014) Limb Redshift of the Fraunhofer Lines in the Solar Spectrum.